Dalton Transactions

PAPER

View Article Online
View Journal | View Issue

Cite this: *Dalton Trans.*, 2014, **43**, 7924

Fabrication and catalytic activity of FeNi@Ni nanocables for the reduction of *p*-nitrophenol†

Linyi Zhou,[a] Ming Wen,*[a,b] Qingsheng Wu[a] and Dandan Wu[a]

Received 7th January 2014,
Accepted 25th February 2014

DOI: 10.1039/c4dt00052h

www.rsc.org/dalton

Magnetic FeNi@Ni nanocables were prepared as a superior recyclable catalyst towards the hydrogenation reduction of *p*-nitrophenol to *p*-aminophenol through a two-step tunable assembly process in a solvothermal system. The proposed fabrication mechanism was verified through characterization by SEM, TEM, XRD, XPS, and UV-Vis. The as-prepared FeNi@Ni nanocomposites are core–shell-structured nanocables with Ni nanoparticles (NPs) attached on FeNi nanorods (NRs) surface loosely. The catalytic reactivity monitored by means of a UV-vis dynamic process shows FeNi@Ni nanocables can catalyse the transformation of *p*-nitrophenol to *p*-aminophenol completely under an ambient atmosphere at room temperature, and enable the catalysis to be more efficient than its counterparts FeNi NRs and Ni NPs due to the interfacial synergistic effect. Additionally, the resultant hierarchical metal–alloy nanocomposites possess ferromagnetic behaviour, and can be easily separated and recycled by an external magnet field for application.

Introduction

p-Nitrophenol (PNP) as a refractory toxic contaminant in industrial wastewater is otherwise the raw material for the synthesis of *p*-aminophenol (PAP), which is of great importance in the pharmaceutical and dye industries as a potent intermediate.[1–5] Hence great attention has been paid to the reduction of PNP to PAP. The manufacturing technique has evolved from the traditional multi-step iron/acid reduction/catalytic process[6–8] to a green direct catalytic hydrogenation reduction route[9] due to its environmental friendliness, atomic efficiency, and compatibility in industrial processes. That is to say, highly-active catalysts with good selectivity are required in the transformation process.

Nanosized noble metal catalysts, such as Au, Ag, Pt/C,[9] Pt–Au nanocrystals,[10] Pd-based nanostructures[11] and so on, show superior intrinsic activity, but their non-selectivity leads to undesired by-products and difficult purification.[12–14] On the other hand, non-noble metallic nanocatalysts with higher selectivity[15] for hydrogenation require a high reaction temperature and a high pressure because of their lower intrinsic activity.[16,17] Thus, nanoalloys including noble metals can possess superior activity together with a high selectivity for significant catalytic reactions. Up to now, noble metal contained bimetallic nanocatalysts used in the hydrogenation of PNP have been developed to be multifunctional[18] with multi-dimension,[19] multi-morphologies[20] and multi-components,[21] because their excellent catalytic activities with high selectivity[19] can be induced by the synergistic interaction between noble and non-noble metallic components, large surface areas and dispersed active sites. However, the extensive use of noble metal has raised concerns regarding the high cost with low usage effectiveness. Therefore, this remains a large obstacle to be overcome for harvesting low cost metallic nanocatalysts with high activity.

To accomplish this target, we have designed a noble-metal-free core–shell-structured FeNi@Ni nanocables catalyst. Because Ni nanocatalyst exhibits good catalytic selectivity in hydrogenation reactions,[20] such as Ni/AC (activated carbon),[22] NiCo nanoalloys.[21] Moreover, the diameter of Fe approaches that of Ni, hence Fe can easily form an alloy with Ni,[23] and can lead to a continuously adjustable catalytic activity since suitable amounts of Fe dissolved in FeNi catalysts could contribute to the dispersion of active sites of Ni. So inexpensive magnetic elements of Fe and Ni were selected to fabricate FeNi NRs as the core, Ni NPs were attached on the surface of FeNi NRs forming a loose shell of the desired FeNi@Ni nanocables. Offering a large amount of macropores with a large surface area, this kind of structure can greatly facilitate reactant diffusion and transportation in the catalytic reaction performance. Therefore, the desired catalytic activity can be notably exhibited toward the hydrogenation reduction of PNP under an ambient atmosphere at room temperature (r.t.), because

[a]*Department of Chemistry, State Key Laboratory of Pollution Control and Resource Reuse, Tongji University, Shanghai 200092, China*
[b]*Shanghai Key Lab Development & Application Metal Function Material, Tongji University, Shanghai, China. E-mail: m_wen@tongji.edu.cn; Fax: +86-21-65981097*
† Electronic supplementary information (ESI) available: Further SEM images, UV-vis spectra, magnetic data. See DOI: 10.1039/c4dt00052h

the metallic interfaces of Fe/Ni and Ni/Ni can accelerate electronic transmission and the loose Ni NPs shell facilitates the diffusion and transmission of reactants and products.[18] Furthermore, the magnetic property, proposed catalytic mechanism and the rate of reaction were also investigated for FeNi@Ni core–shell nanocables in detail in the present work.

Experimental chemicals

Ferric oxalate ($Fe_2(C_2O_4)_3{\cdot}5H_2O$, 99%), nickel acetate tetrahydrate ($Ni(CH_3COO)_2{\cdot}4H_2O$, 99%), nickel chloride hexahydrate ($NiCl_2{\cdot}6H_2O$, 99%), polyvinylpyrrolidone K-30 (PVP, $(C_6H_9NO)_n$, M_w: av. 40 000), sodium borohydride ($NaBH_4$, 96%), sodium hydroxide (NaOH, 96%), ethanol (C_2H_5OH, 99%), ethanol (C_2H_5OH, 75%) and ethylene glycol ($C_2H_6O_2$, 99.7%) were purchased from Sinopharm Chemical Reagent Co., Ltd (SCRC). *p*-Nitrophenol ($C_6H_5NO_3$, PNP, 99%) was purchased from Aladdin. All the reagents were used without further purification.

Synthesis of FeNi NRs

The FeNi NRs were prepared in a solvothermal reaction system. The synthesis process of $Fe_{57}Ni_{43}$ NRs are described as follows: Fe^{3+} aqueous solution (16 mL, 5 mM) was mixed with Ni^{2+} ethylene glycol solution (4 mL, 20 mM) in a Teflon-lined stainless steel autoclave at r.t. Then, 55 mL ethylene glycol was injected, followed by ultrasonic treatment for half an hour. The reaction system was sealed and heated at a heating rate of 1 °C min^{-1} from r.t. to 180 °C, and kept for 12 h. After the reaction was cooled to r.t., the products were collected from the bottom of the container. The as-synthesized FeNi NRs were alternately washed by ethanol and deionized water under ultrasonic centrifugation over three times, then dried in a vacuum oven for further synthesis of FeNi@Ni nanocables.

Synthesis of FeNi@Ni nanocables

Typically, $Fe_{57}Ni_{43}$ NRs (5 mg) were mixed with 40 mg NaOH, 25 mg PVP and 10 mL $C_2H_6O_2$ in the autoclave, then $NiCl_2{\cdot}6H_2O$ (1 mL, 20 mM) was injected into the autoclave. After completely being dissolved by ultrasonication, the reaction system was allowed to stand for about 3 h. Then the system was sealed and heated at a heating rate of 1 ~ 5 °C min^{-1} from r.t. to 180 °C, and kept for 12 h. After the reaction was cooled to r.t., the FeNi@Ni nanocables were collected at the bottom of the container. The products were alternately washed by ethanol and deionized water under ultrasonication three times, then dried in a vacuum oven for the following experiment.

Characterization

The morphology and structure of the products were identified by field-emission scanning electron microscopy (FE-SEM, JEOLS-4800, Japan), transmission electron microscopy (TEM, JEOL JEM-1200EX microscope, Japan). The chemical composition was carried out by selected area energy dispersive spectroscopy (EDS) conducted at 20 keV on a TN5400 EDS instrument (Oxford). The structural information on the samples was collected by X-ray powder diffraction (XRD) measurements performed on a Bruker D8 (German) X-ray diffractometer with a Cu Kα radiation source (λ = 0.154056 nm). XPS experiments were carried out on a RBD upgraded PHI-5000C ESCA system (Perkin Elmer) with Mg K radiation (h = 1253.6 eV) or Al K radiation (h = 1486.6 eV). The whole spectra (0 ~ 1100 (1200) eV) and the narrow spectra of all the elements with a much higher resolution were both recorded by using a RBD 147 interface (RBD Enterprises, USA) through the AugerScan 3.21 software. Binding energies were calibrated by using the containment carbon (C1s = 284.6 eV). The data analysis was carried out by using the RBD AugerScan 3.21 software provided by RBD Enterprises or XPSPeak4.1 provided by Raymund W. M. Kwok (The Chinese University of Hong Kong, China). The Lakeshore 735 vibration sample magnetometer (VSM) (America) was used to measure the magnetic properties. The UV-Vis spectra of the samples (dispersed into 75% ethanol) were measured on an Agilent-8453 ultraviolet visible spectrophotometer.

Evaluation of catalytic activity

To characterize the catalytic performance of FeNi@Ni nanocables, hydrogenation reduction of PNP to PAP in aqueous solution by a large excess of $NaBH_4$ was used as a model reaction. In contrast, the as-prepared FeNi NRs and Ni NPs were also investigated to compare the catalytic activity. The UV-Vis dynamic measurement was carried out in a standard quartz cuvette, with a 1 cm path and 3 mL volume. First, catalysts (3 mg) were introduced to the reactor containing 2 mL of freshly prepared 75% C_2H_5OH solution of PNP (1 mM) with magnetic stirring at r.t. and 17 mg $NaBH_4$ was then added into the solution. Time-dependent absorption spectra were recorded in the UV-Vis spectrophotometer over a scanning range from 250 to 550 nm every 15 s. During the reaction, a good number of H_2 bubbles were released into the solution, and the colour of the solution began changing from light yellow to colourless.

Results and discussion

Fabrication mechanism

The core–shell FeNi@Ni nanocables were fabricated based on $Fe_{57}Ni_{43}$ NRs (Fig. 2A) through a two-step controlling assembly process in a solvothermal system,[24] where Ni NPs attached on the FeNi NRs surface loosely, as shown in Fig. 1. The well dispersed FeNi NRs were generated through reducing the same amount of $Fe_2(C_2O_4)_3{\cdot}5H_2O$ and $Ni(CH_3COO)_2{\cdot}4H_2O$ by ethylene glycol in a surfactant-free chemical reaction system *via* a small temperature gradient (1 °C min^{-1}) from r.t. to 180 °C for 12 h. Under the high pressure atmosphere, the FeNi NRs were constructed by an anisotropic cubic crystalline structure of FeNi.[25] FeNi@Ni nanocables were obtained in the second step based on FeNi NRs, the Ni NPs self-assemble on the surface of FeNi NRs in a Teflon-lined stainless steel autoclave at 180 °C

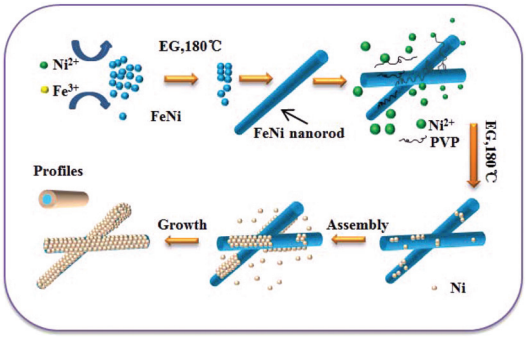

Fig. 1 Schematic illustration of the fabrication process of FeNi@Ni nanocables.

for 12 h. With the appropriate amount of NaOH involved in the reaction, the directional assembly of FeNi@Ni nanocables proceeded *via* reducing $NiCl_2 \cdot 6H_2O$ by ethylene glycol with the application of PVP as surfactant in a Teflon-lined stainless steel autoclave at 180 °C for 12 h. The reaction parameters were optimized by adjusting the covering amount of Ni NPs, concentration of PVP and pH-modifier NaOH (ESI, Fig. S1–S3†). In the presence of NaOH at 1 mM, the concentration of Ni^{2+} at 20 mM resulted in the desired diameter size of FeNi@Ni nanocables, and a higher concentration of Ni^{2+} led to larger diameters.

Morphology and structure

Fig. 2 illustrates the morphology and structure of FeNi@Ni nanocables fabricated through a two-step tunable assembly process in a solvothermal system based on amorphous FeNi NRs with diameters of ~300 nm (Fig. 2A and B). We can observe that the products are nanocables in shape with an average diameter of ~1.25 μm (Fig. 2D), where Ni NPs are loosely attached on the surface of FeNi NRs (Fig. 2E). As shown in Fig. 2F, the TEM image clearly shows core–shell-structured nanocables, where the gray shell is composed of Ni NPs with a

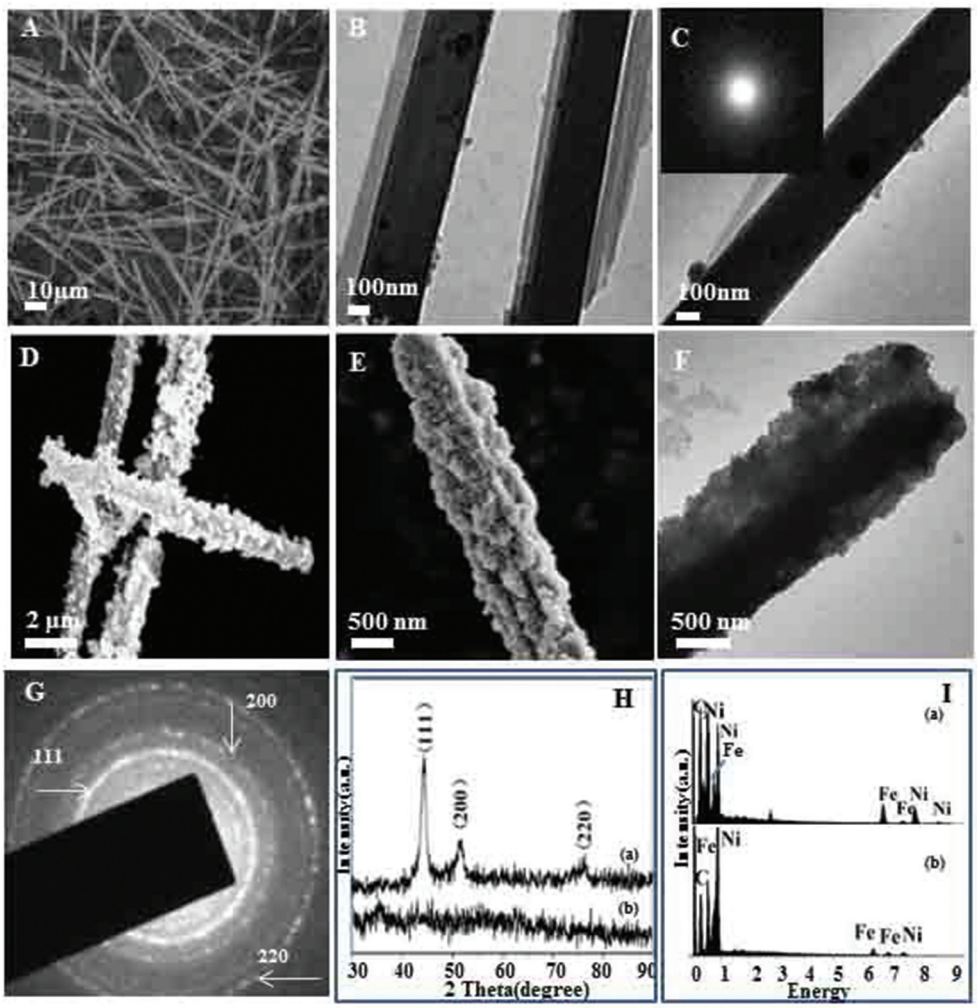

Fig. 2 (A, B) SEM and TEM images of FeNi NRs; (C) TEM image of a single FeNi NRs with inset SADP; (D) SEM image of FeNi@Ni nanocables; (E, F) SEM and TEM images of a single FeNi@Ni nanocables; (G) SADP recorded from a single FeNi@Ni nanocables; (H) XRD of FeNi@Ni nanocables (a) and FeNi NRs (b); (I) EDS of FeNi@Ni nanocables (a) and FeNi NRs (b).

thickness of ~475 nm and the dark core is FeNi NRs with a diameter of ~300 nm. The core–shell cable structure can also be further verified by the selected-area electron diffraction pattern (SADP) from a single FeNi core NR and FeNi@Ni nanocable, respectively. In the inset of Fig. 2C, the SADP of FeNi NRs exhibits a diffuse halo indicating its amorphous structure, while FeNi@Ni nanocables present a clear crystalline ring spot (Fig. 2G), which corresponds to the polycrystalline structure with the indexed plane of (111), (200), (220), suggesting that Ni is isolated as NPs assembling around the surface of the FeNi NRs. Thus, the fabricated products are core–shell-structured FeNi@Ni nanocables. In Fig. 2H, the XRD pattern of FeNi NRs (curve (b)) presents one broad halo at 45° corresponding to a face-center cubic (fcc) structure with a random crystalline orientation,[26] confirming the chemical disorder amorphous structure, which is consistent with the SADP in the inset of Fig. 2C. After annealing at 773 K under argon, the phase transfers to a long-range chemically ordered fcc structure of FeNi alloy (JCPDF#38-0419), which was evidenced by the XRD pattern shown in Fig. S4.† However, the XRD pattern of FeNi@Ni nanocables agrees well with the fcc structure of Ni (JCPDF#38-0419), and corresponds to the SADP in Fig. 2G. This further confirmed the structure of FeNi@Ni nanocables.

The EDS analysis carried out on the as-prepared FeNi NRs and FeNi@Ni nanocables are illustrated in Fig. 2I. It undoubtedly reveals that the products of FeNi NRs contain Ni and Fe in a molar ratio of ~1 : 1(curve (b)), while the Ni/Fe molar ratio of FeNi@Ni nanocables increases to ~4 : 1 (curve (a)). All the characterization above exhibits the formation of core–shell-structured FeNi@Ni nanocables.

X-ray photoelectron spectroscopy (XPS) in the region of 0–1000 eV was applied to characterize the last atomic layer of products, and shown in Fig. 3. In Fig. 3A and 3D, the four photoemission peaks (O1s, Fe2p, Ni2p, C1s) are observed in XPS spectra for the surface of FeNi NRs and FeNi@Ni nanocables, respectively. The magnified Fe2p peaks consisting of two sharp peaks are respectively located at 710.14 eV and 720.53 eV due to the spin–orbit splitting of $2p_{3/2}$ and $2p_{1/2}$ (Fig. 3B and E), the detailed spectrum of Ni2p peaks are located at 858.45 eV and 870.43 eV (Fig. 3C and F), which are due to the spin–orbit doublet splitting of $2p_{3/2}$ and iron. An enhancement of the Ni2p peak with the weakness of C1s and O1s is observed in Fig. 3D compared with that of FeNi NRs (Fig. 3A) showing that there are Ni NPs covering the surface of FeNi NRs, which can further confirm the structure of the products. The O1s peak located at 531.87 eV indicates that both the surface of FeNi NRs and FeNi@Ni nanocables can be oxidized by oxidizing substances in the air. We can also find the Fe2p peak in Fig. 2D probably because that FeNi NRs are not fully covered by Ni NPs.

Magnetic property

The magnetic behaviors of FeNi@Ni nanocables, Ni NPs and FeNi NRs were investigated by VSM at r.t. and summarized in ESI in Table S1.† The magnetic hysteresis loop is plotted in Fig. 4. The magnetization saturation (M_s) value of FeNi@Ni nanocables is 156.82 emu g^{-1}, which is higher than that of FeNi NRs (29.75 emu g^{-1}) due to the Ni NPs surrounding the magnetic FeNi NRs providing more magnetic moment per unit mass than that of the ferromagnetic core regions. It promotes the magnetic-recyclability of products. In our case, the as-prepared FeNi@Ni nanocables, suspended in aqueous solution, can quickly respond to a magnet (Fig. 4C), and then can be readily redispersed in water by stirring or sonication due to its low coercivity (H_c) (48.42 Oe) and retentivity (M_r) (11.86 emu g^{-1}), indicating the excellent ability of the magnetic separation.

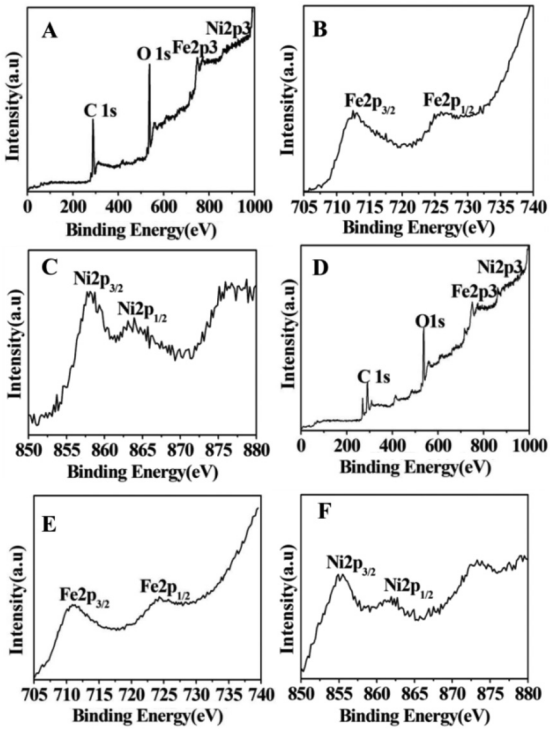

Fig. 3 XPS spectra of FeNi NRs (A) with detailed spectra of Fe2p (B) and Ni2p (C); XPS spectra of FeNi@Ni nanocables (D) with detailed spectra of Fe2p (E) and Ni2p (F).

Catalytic activity

Because PNP is a refractory toxic contaminant in industrial wastewater, while PAP is an important intermediate for the pharmaceutical and dyeing industries,[1–5] and Ni included catalysts are generally employed for the reduction of PNP to PAP. It is known that the catalyst could lower the activation energy of this reaction to accelerate electron transfer from donor BH^{4-} to acceptor PNP.[27] Hence, the catalytic activities of the as-obtained FeNi@Ni nanocables and FeNi NRs as well as Ni NPs were evaluated toward the hydrogenation reduction of PNP to PAP by employing excess $NaBH_4$ as a model reaction under an ambient atmosphere at r.t. In the reaction, the initial concentrations of PNP and $NaBH_4$ were kept at 0.1 mM and 0.45 mM, respectively, and were monitored by UV-Vis spectra. This pseudo-first-order reaction,[28] which is famous for its simple, green process with fast speed in the presence of metallic

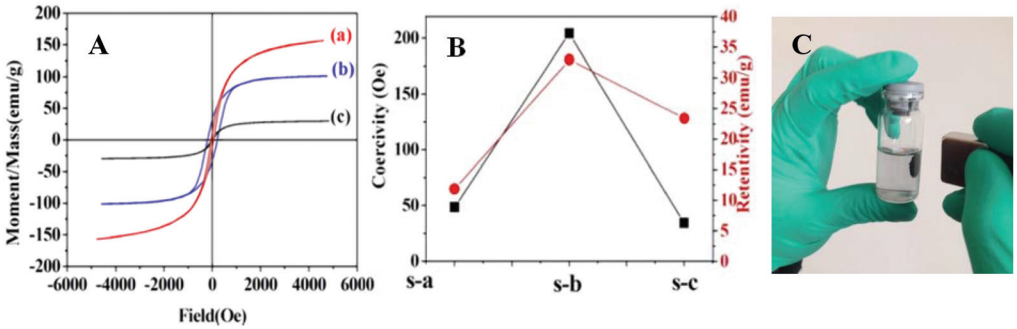

Fig. 4 Magnetic behaviors: (A) room-temperature hysteresis loops of FeNi@Ni nanocables (a), Ni NPs (b) and FeNi NRs(c). (B) The variations of coercivity (H_c) and retentivity (M_r) of FeNi@Ni nanocables (S-a), Ni NPs (S-b) and FeNi NRs (S-c). (C) The photo of FeNi@Ni nanocables shows the quick response to a magnet.

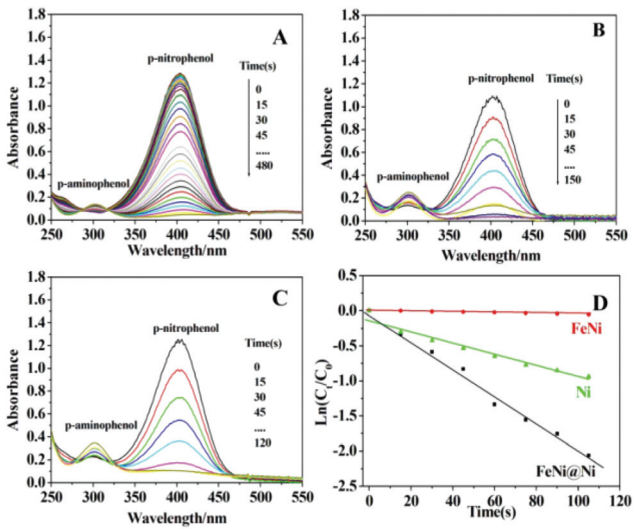

Fig. 5 UV-vis spectra of reaction solutions containing different catalysts: (A) FeNi NRs; (B) Ni NPs; (C) FeNi@Ni nanocables; (D) plots of $\ln(C_t/C_0)$ *versus* time for the catalytic reduction of *p*-nitrophenol at r.t. with FeNi@Ni nanocables; Ni NPs; FeNi NRs.

surfaces only based on the excess $NaBH_4$ in the reaction, therefore the BH_4^- concentration remained essentially constant throughout the reaction.

Fig. 5 shows the catalytic activities of FeNi@Ni nanocables and their counterparts (FeNi NRs and Ni NPs). A clear spectral profile with an absorption maximum at 400 nm in ethanol solution for PNP can be observed.[27] The blank experiments were carried out in order to exclude the possibility of the reduction generated in the absence of catalyst. There was no variation in peak intensity at 400 nm with the prolonging of time, indicating that the reduction did not take place without a catalyst being involved in the reaction (ESI, Fig. S5†). However, a small amount of prepared Ni included catalysts caused fading and final bleaching of the yellow color of PNP in succession, demonstrating the generation of a reduction reaction. During the reaction process, the absorption peak at 400 nm was gradually weakened, which was accompanied by a gradual absorbance enhancement of a new peak at 300 nm, corresponding to the formation of PAP (Fig. 5). As shown in Fig. 5A–C, on addition of FeNi@Ni nanocables, FeNi NRs or Ni NPs, a successive absorption spectra of PNP at 400 nm was observed by UV-vis. Comparing Fig. 5A and B, when FeNi@Ni nanocables were added to the reaction solution as catalysts, the absorption peak at 400 nm can dramatically decrease in intensity in 120 s. A sharp acceleration of the reaction rate can also be observed through the values of the rate constants of the above catalytic reactions which were calculated from the plot of $\ln(C_t/C_0)$ *versus* time t (Fig. 5D) (where C_0 and CT represent the initial concentration and the concentration at time t of PNP, respectively; C_t/C_0 is measured from the relative intensity of absorbance at 400 nm). It is clear to understand that FeNi@Ni nanocables exhibit the highest catalytic activity for the hydrogenation reduction of PNP to PAP. Additionally, there was an isosbestic point shown in thee UV-vis spectra, indicating that only two principal species, PNP and PAP, in the reaction, so PNP was only transformed to PAP without any other by-product.[29–32] And the conversion can be calculated from the UV-vis data. In this work, the conversion is 91.4%.

For industrial application, catalytic cycles as a typical index to measure the reusability and recoverability of catalysts were used to test the as-synthesized FeNi@Ni in the nitro reduction.[33] Fig. S6† shows seven cycles of the catalytic reaction transforming PNP to PAP, in the first 5 recycle, PNP can be successfully reduced to PAP with a stable conversion efficiency of almost 100%. The catalysts can be easily collected by an external magnet and washed by deionized water after reaction. The reaction rate decreased as the cycles increase and this was probably because of the loss of FeNi@Ni catalysts during the separation process as well as the decrease of catalytic activity. Additionally, structure stability of FeNi@Ni nanocables in the hydrogenation reduction of PNP in $NaBH_4$ ethanol aqueous under an ambient atmosphere at room temperature has also been tested, SEM images of FeNi@Ni nanocables after the hydrogenation reduction of PNP to PAP two times and seven times are shown in Fig. S7(A) and S7(B),† respectively. FeNi@Ni nanocables basically maintain the original structure, indicating the structure stability of FeNi@Ni nanocables in 75% ethanol solution.

Conclusions

In summary, new-design magnetic FeNi@Ni hierarchical nanocables have been successfully fabricated through a two-step tunable assembly process in solvothermal system. Owing to the synergistic effect of interfacial and plasma resonance effect as well as the magnetic property, the FeNi@Ni nanocables exhibit superior catalytic activity and recycling efficiency toward the hydrogenation reduction of PNP to PAP under ambient atmosphere at r.t. The self-assembly strategy synthesizing the desired morphologies and structures with exposed active sites provides a method to prepare hierarchical nanostructures, which have a great potential for extension to other metallic systems in the application of catalytic reduction of other aromatic hydrocarbon pollutants.

Acknowledgements

This work is financial supported by National Natural Science Foundation (no. 21171130, 51271132, 91122025, and 91222103) and 973 Project (no. 2011CB932404) from China.

Notes and references

1 Y. Du, H. L. Chen, R. Z. Chen and N. P. Xu, *Appl. Catal., A*, 2004, **277**, 259–264.
2 Y. Lu, Y. Mei and M. Ballauff, *J. Phys. Chem. B*, 2006, **110**, 3930–3937.
3 C. V. Rode, M. J. Vaidya, R. Jaganathan and R. V. Chaudhari, *Chem. Eng. Sci.*, 2001, **56**, 1299–1304.
4 M. J. Vaidya, S. M. Kulkarni and R. V. Chaudhari, *Org. Process Res. Dev.*, 2003, **7**, 202–208.
5 Z. Jiang, J. Xie, D. Jiang, J. Jing and H. Qin, *CrystEngComm*, 2012, **14**, 4601–4611.
6 S. Saha, A. Pal, S. Kundu, S. Basu and T. Pal, *Langmuir*, 2010, **26**, 2885–2893.
7 M. L. Crossley, *J. Ind. Eng. Chem.*, 1922, **14**, 802–804.
8 S. P. Bawane and S. B. Sawant, *Appl. Catal., A*, 2005, **293**, 162–170.
9 C. V. Rode, M. J. Vaidya and R. V. Chaudhari, *Org. Process Res. Dev.*, 1999, **3**, 465–470.
10 S. Y. Song, R. X. Liu, Y. Zhang, J. Feng, D. P. Liu, Y. Xing, F. Y. Zhao and H. J. Zhang, *Chem.–Eur. J.*, 2010, **16**, 6251.
11 H. P. Rong, S. F. Cai, Z. Q. Niu and Y. D. Li, *ACS Catal.*, 2013, **3**, 1560–1563.
12 Z. D. Pozun, S. E. Rodenbusch, E. Keller, K. Tran, W. J. Tang, K. J. Stevenson and G. Henkelman, *J. Phys. Chem. C*, 2013, **117**, 7598–7604.
13 S. F. Cai, H. H. Duan, H. P. Rong, D. S. Wang, L. Li and Y. D. Li, *ACS Catal.*, 2013, **3**, 608–612.
14 H. Wang, Z. X. Dong and C. Z. Na, *ACS Sustainable Chem. Eng.*, 2013, **1**, 746–752.
15 S. F. Cai, H. H. Duan, H. P. Rong, D. S. Wang, L. S. Li, W. He and Y. D. Li, *ACS Catal.*, 2013, **3**, 608–612.
16 H. Liu, J. Deng and W. Li, *Catal. Lett.*, 2010, **137**, 261–266.
17 A. Corma, P. Serna, P. Concepción and J. J. Calvino, *J. Am. Chem. Soc.*, 2008, **130**, 8748–8753.
18 J. Lee, J. C. Park and H. Song, *Adv. Mater.*, 2008, **20**, 1523–1528.
19 Y. Du, H. L. Chen, R. Z. Chen and N. P. Xu, *Appl. Catal., A*, 2004, **277**, 259–264.
20 Z. F. Jiang, J. M. Xie, D. L. Jiang, X. J. Wei and M. Chen, *CrystEngComm*, 2013, **15**, 560.
21 K. L. Wu, X. W. Wei, X. M. Zhou, D. H. Wu, X. W. Liu, Y. Ye and Q. Wang, *J. Phys. Chem. C*, 2011, **115**, 16268–16274.
22 J. F. Ding, L. G. Chen, R. Shao, J. Wu and W. T. Dong, *React. Kinet., Mech. Catal.*, 2012, **106**, 225–232.
23 Y. W. Chen and N. Sasirekha, *Ind. Eng.Chem. Res.*, 2009, **48**, 6248–6255.
24 B. L. Sun, M. Wen, Q. S. Wu and J. Peng, *Adv. Funct. Mater.*, 2012, **22**, 2860–2866.
25 M. Wen, X. G. Meng, B. L. Sun, Q. S. Wu and X. L. Chai, *Inorg. Chem.*, 2011, **50**, 9393–9399.
26 J. Peng, M. Wen, C. X. Wang, Q. S. Wu and Y. Z. Sun, *Dalton Trans.*, 2013, **42**, 8667–8673.
27 A. Gangula, R. Podila, R. Muddasani, L. Karanam, C. Janardhana and A. M. Rao, *Langmuir*, 2011, **27**, 15268–15274.
28 F. H. Lin and R. A. Doong, *J. Phys. Chem. C*, 2011, **115**, 6591–6598.
29 Q. An, M. Yu, Y. T. Zhang, W. F. Ma, J. Guo and C. C. Wang, *J. Phys. Chem. C*, 2012, **116**, 22432–22440.
30 Y. H. Deng, Y. Cai, Z. K. Sun, J. Liu, C. Liu, J. Wei, W. Li, C. Liu, Y. Wang and D. Y. Zhao, *J. Am. Chem. Soc.*, 2010, **132**, 8466.
31 P. H. Zhang, Y. M. Sui, G. J. Xiao, Y. N. Wang, C. Z. Wang, B. B. Liu, G. T. Zou and B. Zou, *J. Mater. Chem. A*, 2013, **1**, 1632–1638.
32 J. G. Lee, J. C. Park and H. J. Song, *Adv. Mater.*, 2008, **20**, 1523–1528.
33 R. M. Dyson, M. Hazenkamp, K. Kaufmann, M. Maeder, M. Studer and A. J. Zilian, *J. Chemom.*, 2000, **14**, 737.